ICOS and Bcl6-dependent pathways maintain a CD4 T cell population with memory-like properties during tuberculosis

Albanus O. Moguche,[1,2] Shahin Shafiani,[1] Corey Clemons,[1,2] Ryan P. Larson,[1,2] Crystal Dinh,[1] Lauren E. Higdon,[2] C.J. Cambier,[2] James R. Sissons,[1] Alena M. Gallegos,[3] Pamela J. Fink,[2] and Kevin B. Urdahl[1,2]

[1]Seattle Biomedical Research Institute (renamed Center for Infectious Disease Research), Seattle, WA 98109
[2]Department of Immunology, University of Washington School of Medicine, Seattle, WA 98104
[3]Department of Immunology, International Centre for Genetic Engineering and Biotechnology, New Delhi 110067, India

Immune control of persistent infection with *Mycobacterium tuberculosis* (Mtb) requires a sustained pathogen-specific CD4 T cell response; however, the molecular pathways governing the generation and maintenance of Mtb protective CD4 T cells are poorly understood. Using MHCII tetramers, we show that Mtb-specific CD4 T cells are subject to ongoing antigenic stimulation. Despite this chronic stimulation, a subset of PD-1$^+$ cells is maintained within the lung parenchyma during tuberculosis (TB). When transferred into uninfected animals, these cells persist, mount a robust recall response, and provide superior protection to Mtb rechallenge when compared to terminally differentiated Th1 cells that reside preferentially in the lung-associated vasculature. The PD-1$^+$ cells share features with memory CD4 T cells in that their generation and maintenance requires intrinsic Bcl6 and intrinsic ICOS expression. Thus, the molecular pathways required to maintain Mtb-specific CD4 T cells during ongoing infection are similar to those that maintain memory CD4 T cells in scenarios of antigen deprivation. These results suggest that vaccination strategies targeting the ICOS and Bcl6 pathways in CD4 T cells may provide new avenues to prevent TB.

CORRESPONDENCE
Kevin B. Urdahl:
kevin.urdahl@cidresearch.org

Abbreviations used: Ag85B, *Mycobacterium tuberculosis* antigen 85B; BCG, Bacille Calmette-Guerin; ESAT-6, Early secreted antigenic target 6 kD; Mtb, *M. tuberculosis*; MVA85A, modified vaccine Ankara vector expressing *M. tuberculosis* antigen 85A; TB, tuberculosis.

Despite over 80 years of global immunization with attenuated *Mycobacterium bovis* Bacille Calmette-Guerin (BCG), TB remains a massive international health emergency, with ∼9 million new cases of active disease and over a million deaths annually (WHO, 2014). Although BCG vaccination confers limited protection against disseminated infection in children, its efficacy wanes over time and confers little or no protection in adults (Andersen and Woodworth, 2014). An effective vaccine is urgently needed, but achieving this goal has proven elusive. This difficulty was recently highlighted by the completion of the first efficacy trial for a TB vaccine since BCG itself was tested (Tameris et al., 2013). The vaccine, a modified vaccinia Ankara vector expressing Mtb antigen 85A (MVA85A), was used to boost infants previously immunized with BCG, but provided no protection beyond the very limited immunity conferred by BCG alone. This failure occurred despite the fact that MVA85A achieved its goal of amplifying the Mtb-specific T cell population in blood (Scriba et al., 2011).

Striving to increase the number of Mtb-specific Th1 cells (CD4 T cells capable of producing the immune modulatory cytokine IFN-γ), a strategy shared by most TB vaccine candidates currently in human trials, is rationalized because these cells are clearly critical for protective immunity. Mice lacking CD4 T cells, IFN-γ, IL-12 signaling (a pathway required for Th1 development), or T-bet (a transcription factor requisite for Th1s) are profoundly susceptible to Mtb infection (Cooper, 2009). Likewise, humans with genetic deficiencies in IFN-γ or IL-12 signaling (Fortin et al., 2007), as well as HIV-infected individuals depleted of CD4 T cells (Deffur et al., 2013), are severely restricted in their ability to contain mycobacterial infections, including TB. Unfortunately, the frequency of

The Rockefeller University Press $30.00
J. Exp. Med. 2015 Vol. 212 No. 5 715–728
www.jem.org/cgi/doi/10.1084/jem.20141518

Mtb-specific Th1 cells in the blood and lymphoid periphery of mice and humans does not correlate with protection against TB (Leal et al., 2001; Elias et al., 2005; Fletcher, 2007; Mittrücker et al., 2007; Urdahl et al., 2011; Urdahl, 2014).

The discrepancy between the fact that Th1 cells are critical for TB immunity, yet higher numbers of these cells do not necessarily confer greater protection, could potentially be explained if subsets of Mtb-specific Th1 CD4 T cells differ in their ability to control Mtb infection. Mtb-specific CD4 T cells are not homogeneous, but in mice can be separated into functionally distinct subsets that express either KLRG1 or PD-1 (Reiley et al., 2010). Mtb-specific CD4 T cells expressing KLRG1 exhibit a heightened capacity to produce proinflammatory cytokines, such as IFN-γ and TNF. These cells represent terminally differentiated Th1 cells because, upon transfer into a second Mtb-infected host, they proliferate poorly, maintain their KLRG1$^+$ phenotype, and are short-lived. In contrast, PD-1$^+$KLRG1$^-$ cells produce less proinflammatory cytokines than their KLRG1$^+$ counterparts upon restimulation. However, when transferred into infected hosts, they proliferate robustly, are maintained at high numbers, and have the capacity to differentiate into KLRG1$^+$ cells.

There is growing evidence that PD-1$^+$ CD4 T cells mediate superior protection against Mtb than terminally differentiated KLRG1$^+$ Th1 cells. Immunization with BCG induces high numbers of KLRG1$^+$ CD4 T cells, but these cells are short-lived and protection wanes with time (Lindenstrøm et al., 2013). However, immunizations that target subdominant Mtb epitopes (Woodworth et al., 2014), or use a liposomal adjuvant (Lindenstrøm et al., 2013), preferentially expand Mtb-specific CD4 T cells that are KLRG1$^-$ and produce IL-2 and confer superior and longer lasting immunity. Furthermore, adoptive transfer of CD4 T cells resident in the Mtb-infected lung parenchyma (primarily PD-1$^+$ KLRG1$^-$ cells) confers greater protection against Mtb challenge than transfer of CD4 T cells that reside in the lung-associated vasculature (almost exclusively KLRG1$^+$ cells; Sakai et al., 2014).

Given the emerging importance of PD-1$^+$ KLRG1$^-$ CD4 T cells in mediating and maintaining immunity against Mtb, we sought to more fully define this CD4 subset and to elucidate the molecular pathways that promote its induction and maintenance. We found that Mtb-specific CD4 T cells expressing PD-1 are located in the parenchyma of the infected lung and are subject to chronic antigenic stimulation. They share many features with T follicular helper cells (Tfh) and, despite chronic stimulation, also share properties with memory CD4 T cells. These cells persist following adoptive transfer in uninfected hosts in an ICOSL-dependent manner and can mount a robust recall response. Adoptive transfer studies directly demonstrate that PD-1$^+$ CD4 T cells possess significantly greater protective capacity than their terminally differentiated KLRG1$^+$ counterparts. Their generation requires intrinsic expression of Bcl6, and their maintenance during chronic infection requires intrinsic ICOS signaling. Thus, the molecular pathways maintaining memory CD4 T cells and previously shown to function in scenarios of antigen deprivation (Pepper et al., 2011) are also required to maintain a robust and protective Th1 response in the face of ongoing antigenic stimulation.

RESULTS

Mtb-specific CD4 T cells are subject to chronic antigenic stimulation

We used MHCII tetramers to track and characterize CD4 T cells recognizing an epitope of ESAT-6 (Moon et al., 2009; Shafiani et al., 2010, 2013), an immunodominant CD4 T cell antigen in C57BL/6 (B6) mice and humans (Ravn et al., 1999; Winslow et al., 2003). After infection with a low dose of aerosolized Mtb, mycobacteria replicate robustly and accumulate in the lung until day 21 after infection (Fig. 1 A; Cooper, 2009). Concomitant with the Mtb-specific T cell response, the lung bacterial burden plateaus at ∼10^6 CFU and is maintained at this level for at least 300 d. ESAT-6–specific CD4 T cells can first be reliably detected in the lungs at ∼day 16 after infection, and thereafter rapidly expand in numbers. At day 34 after infection, they comprise up to 10% of the total CD4 T cells in the lungs, peaking at ∼10^6 total cells (Fig. 1 B). After a modest contraction phase, this population plateaus at 3–10 × 10^5 cells until at least day 300. Most ESAT-6–specific (but not CD44^{low}) CD4 T cells recovered from the lungs were Ki67$^+$, suggesting their active division (Fig. 1 C). Consistent with a previous finding that ESAT-6–specific T cells proliferate throughout chronic infection (Reiley et al., 2010), we observed that the percentage of tetramer-binding T cells expressing Ki67 was highest during early infection (∼80% at day 34) and continued to comprise a substantial population even at 300 d (Fig. 1 C). To test the antigen dependence of this proliferation, we transferred carboxyfluorescein succinimidyl ester (CFSE)–labeled ESAT-6–specific T cell receptor transgenic (TCRtg) cells from C7 mice (Gallegos et al., 2008). C7 CD4 T cell responses during in vivo responses to Mtb are dependent on TCR recognition of cognate antigen (Gallegos et al., 2011). The proliferation of transferred C7 CD4 T cells measured by CFSE dilution mirrored our previous results with Ki67 expression in endogenous tetramer-binding cells; proliferation peaked in the first 4 wk but remained at high levels throughout chronic infection. Importantly, the inflammatory milieu induced by Mtb infection did not drive bystander CD4 T cell proliferation, because no division of TCRtg chicken ovalbumin-specific CD4 T cells (Barnden et al., 1998) was observed (Fig. 1 D).

We detected IFN-γ in ESAT-6 tetramer-binding and CD44^{hi} (but not CD44^{low}) CD4 T cells (Fig. 2 A) using intracellular cytokine staining of T cells directly ex vivo without in vitro restimulation (Shafiani et al., 2013). At 16 d after infection, ∼20% of ESAT-6–specific T cells recovered from the lungs produced IFN-γ, and this percentage gradually increased to ∼40% on day 300 (Fig. 2 B). IFN-γ production was dependent on TCR signaling in at least half of these cells because administration of cyclosporine A (CsA; an inhibitor of proximal TCR-mediated signaling; Schreiber and Crabtree, 1992), 4 h before euthanasia blocked IFN-γ production in ∼50% of the cells (Fig. 2 C). Collectively, our results indicate

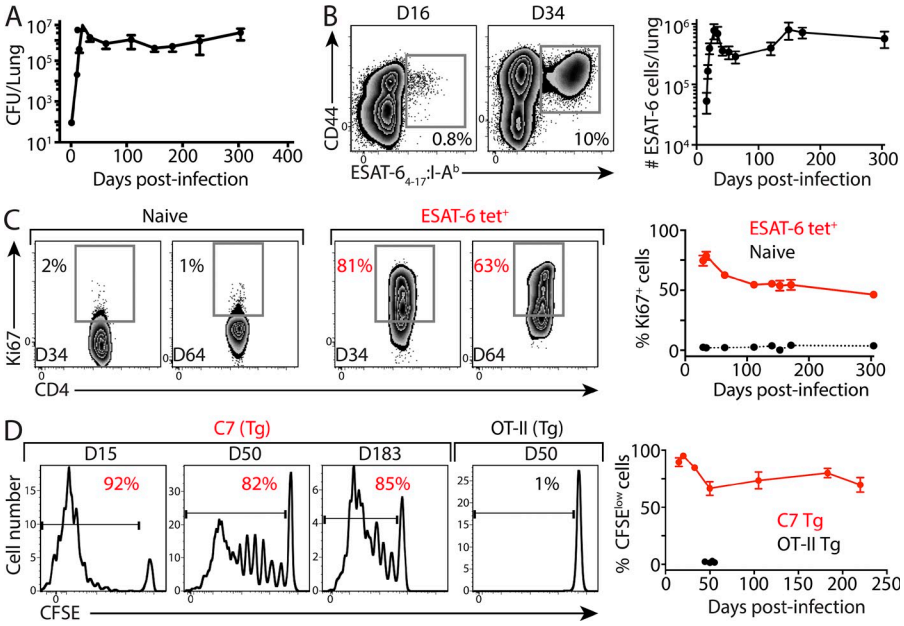

Figure 1. ESAT-6–specific CD4 T cells are subjected to chronic stimulation by antigen. C57BL/6 mice were infected with aerosolized Mtb (~100 CFU/mouse). (A) Lung bacterial loads were assessed by serial plating at the indicated time points. (B) ESAT-6–specific CD4 T cells in the lung were enumerated by flow cytometry. Representative flow cytometry plots and total cell numbers shown. (C) Proportion of Ki67-expressing CD4 T cells among naive CD44^{low} (left) and ESAT-6–specific (right) cells. (D) CFSE-labeled ESAT-6–specific (C7 TCRtg) and ovalbumin-specific (OT-II TCRtg) CD4 T cells were adoptively transferred into Mtb-infected mice at various time points. CFSE dilution was assessed 5 d after transfer, at each of the indicated time points. Data are representative of three independent experiments with three to five mice per group at each time point and cumulative data are represented as mean ± SEM.

that ESAT-6 antigen is readily available for T cell recognition throughout infection and high numbers of ESAT-6–specific T cells are maintained in the lung in the presence of chronic antigenic stimulation.

Mtb-specific CD4 T cells cluster into functionally distinct populations

ESAT-6–specific T cells in the lung can be separated into two distinct populations based on their expression of the inhibitory receptors PD-1 and KLRG1 (Fig. 3 A). Consistent with the findings of a recent report (Reiley et al., 2010), we found that KLRG1$^+$ cells produced more IFN-γ and TNF than their PD-1$^+$ KLRG1$^-$ counterparts after in vitro stimulation with ESAT-6 peptide or anti-CD3 and anti-CD28 antibodies (unpublished data). In contrast, KLRG1$^+$ cells produced very little IL-2, a cytokine almost exclusively produced by a population of polyfunctional PD-1$^+$ KLRG1$^-$ cells that also produced IFN-γ and TNF (Fig. 3 B and not depicted). No TNF

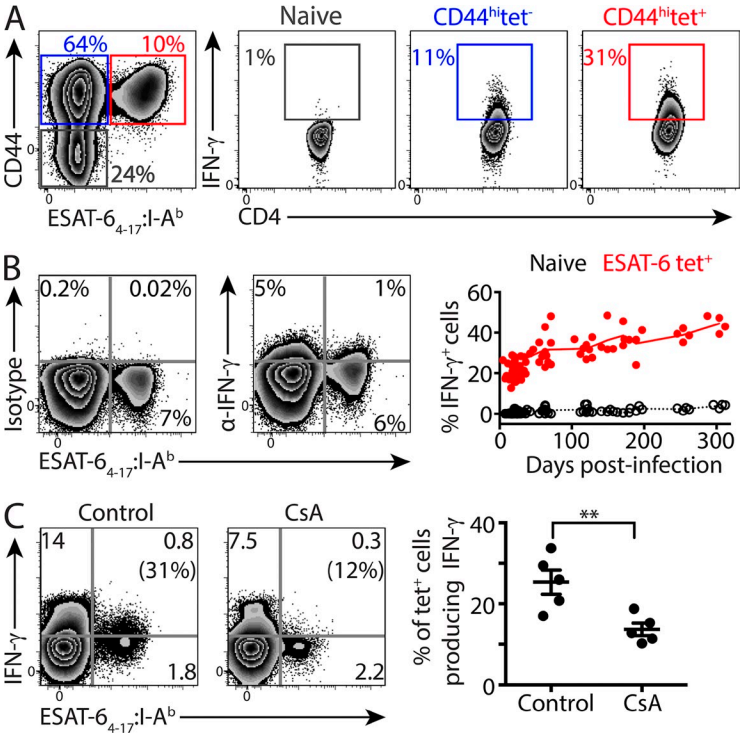

Figure 2. ESAT-6–specific CD4 T cells produce IFN-γ in a TCR signaling–dependent manner. Mice were infected as described in Fig. 1. (A) Intracellular IFN-γ was assessed by flow cytometry directly ex vivo using lung cells (150 d after infection) processed in the presence of Brefeldin A. Gating strategy and representative flow cytometry plots for naive CD44^{low} (gray), nontetramer-binding CD44^{hi} (blue), and ESAT-6 tetramer-binding CD44^{hi} (red) CD4 T cells are shown. (B) Flow cytometry plots show intracellular IFN-γ, or staining with isotype matched control, in ESAT-6–specific CD4 T cells (70 d after infection). Graph shows the percentage of ESAT-6 tetramer-binding or naive CD44^{low} T cells producing IFN-γ at the indicated time points. (C) Mice infected with Mtb 35 d prior were treated intraperitoneally with either cyclosporine-A (CsA) or vehicle, and ESAT-6–specific cells in the lung were assessed for intracellular IFN-γ as in A and B. Numbers in parentheses represent the percentage of ESAT-6 tetramer-binding CD4 T cells producing IFN-γ and the graph shows this value for each mouse and the mean ± SEM for each group. Significance was determined by two-tailed Student's *t* test (**, $P < 0.01$). Data are representative of two independent experiments with four to five mice per group.

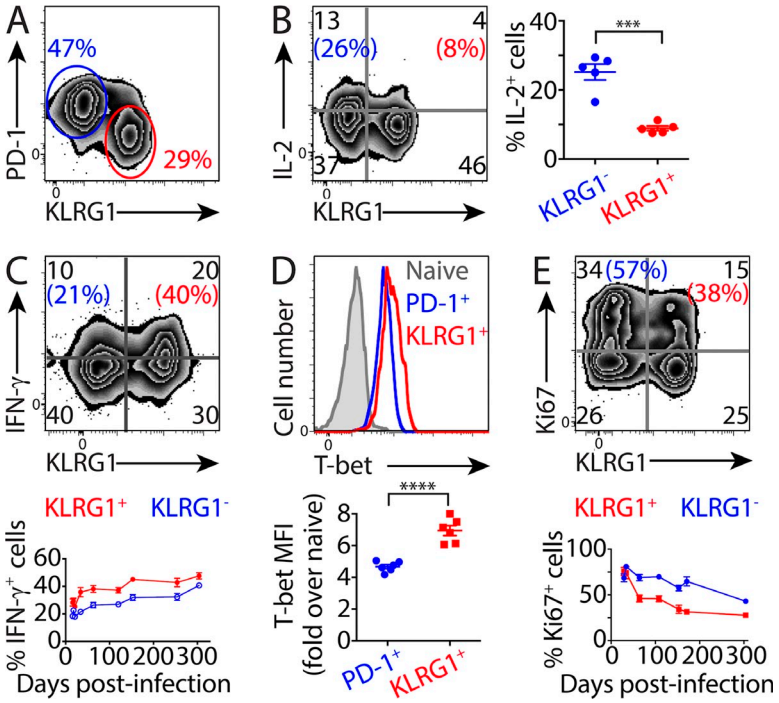

Figure 3. ESAT-6–specific CD4 T cells cluster into distinct functional subsets. Mice were infected as described in Figure 1 and lung CD4 T cells were analyzed by flow cytometry. (A) Representative flow cytometry plot depicts KLRG1 and PD-1 expression by ESAT-6 tetramer-binding CD4 T cells in the lung 90 d after infection. (B) Single-cell suspensions from the lungs of Mtb-infected mice (150 d after infection) were stimulated with ESAT-6_{4-17} in vitro and intracellular cytokine staining was performed. A representative flow plot depicts KLRG1 and IL-2 expression within CD4 T cells coproducing IFN-γ and TNF (gate not depicted), and numbers in parentheses represent the percentage of KLRG1$^-$ (blue) and KLRG1$^+$ (red) cells within this population that express IL-2. The graph shows this value for each mouse and the mean ± SEM for each group. (C) Flow cytometry plot shows direct ex vivo intracellular IFN-γ versus KLRG1 expression for ESAT-6 tetramer-binding CD4 T cells 34 d after infection. Numbers in parentheses denote the percentage of KLRG1$^-$ (blue) or KLRG1$^+$ (red) cells, and the graph below shows the mean ± SEM of these values for each group at various time points after infection. (D) Flow cytometry histograms show T-bet expression by naive CD44^{low} (gray), PD-1$^+$KLRG1$^-$ (blue), and PD-1$^-$KLRG1$^+$ (red) ESAT-6 tetramer-binding CD4 T cells 90 d after infection. Graph below shows the T-bet mean fluorescent intensity (MFI) for each T cell subset in individual mice, and the mean ± SEM for each group. (E) Flow cytometry plot shows Ki67 versus KLRG1 expression for ESAT-6 tetramer-binding CD4 T cells 70 d after infection. Numbers in parentheses denote the percentage of KLRG1$^-$ (blue) or KLRG1$^+$ (red) cells that express Ki67 and the graph below shows the mean ± SEM of these values for each group at various time points after infection. Significance was determined by two-tailed Student's *t* test (***, $P < 0.001$; ****, $P < 0.0001$). Data are representative of three independent experiments with three to five mice per group at each time point.

or IL-2 staining was detected in lung T cells using the direct ex vivo approach. However, consistent with the in vitro restimulation data, a higher percentage of KLRG1$^+$ than PD-1$^+$ KLRG1$^-$ CD4 T cells within the tetramer-binding population produced IFN-γ when assessed immediately after isolation from the lung (Fig. 3 C). Furthermore, KLRG1$^+$ cells expressed high levels of the Th1-defining transcription factor T-bet, whereas PD-1$^+$KLRG1$^-$ cells had intermediate T-bet levels (Fig. 3 D). We also found that PD-1$^+$KLRG1$^-$ ESAT-6–specific CD4 T cells exhibited more proliferation (assessed by Ki67 expression) than KLRG1$^+$ cells at time points beyond day 28 after infection (Fig. 3 E). Overall, these results indicate KLRG1$^+$ cells comprise the primary ESAT-6–specific CD4 T cell population producing IFN-γ in vivo, but PD-1$^+$ cells have a higher capacity to produce IL-2 and undergo more extensive proliferation.

Mtb-specific PD-1$^+$ CD4 T cells share phenotypic features with T follicular helper (Tfh) cells and reside within the lung parenchyma

Because Mtb-specific PD-1$^+$ CD4 T cells represent a self-renewing progenitor population that plays a central role in protective immunity to TB (Reiley et al., 2010), we sought to characterize these cells more extensively. Most PD-1$^+$ ESAT-6–specific CD4 T cells co-expressed the inducible co-stimulatory molecule (ICOS) and CD69, whereas a smaller fraction co-expressed the chemokine receptor CXCR5 and the T and B cell activation marker GL7 (Fig. 4 A). In contrast, tetramer-binding KLRG1$^+$ T cells did not express these markers. To determine whether ESAT-6–specific CD4 T cells were located in the lung parenchyma or the lung-associated vasculature, fluorophore-conjugated T cell–specific antibodies were intravenously injected into mice shortly before euthanasia. This technique accurately labels cells resident in the lung vasculature, including during Mtb infection, and does not label those within the lung parenchyma (Anderson et al., 2014; Sakai et al., 2014). Consistent with the findings of a recent report (Sakai et al., 2014), we found that the vast majority of ESAT-6–specific PD-1$^+$KLRG1$^-$ cells (>95%), but only ∼30–50% of the PD-1$^-$KLRG1$^+$ cells, were resident in the lung parenchyma (Fig. 4 B). Thus, PD-1$^+$ Mtb-specific T cells share phenotypic features with Tfh cells and are located in the lung parenchyma. In contrast, at least 50% of the terminally differentiated KLRG1$^+$ Th1 cells reside within the lung-associated vasculature.

Mtb-specific PD-1$^+$ CD4 T cells survive in the absence of antigenic stimulation

Although PD-1$^+$ Mtb-specific CD4 T cells have Tfh-like features, further analysis of cell surface and intracellular molecules revealed a mixed profile, with expression of both effector and memory markers (Fig. 5 A). CD62L expression reflected an effector phenotype and was low in both PD-1$^+$KLRG1$^-$ and PD-1$^-$KLRG1$^+$ tetramer-binding populations. Although

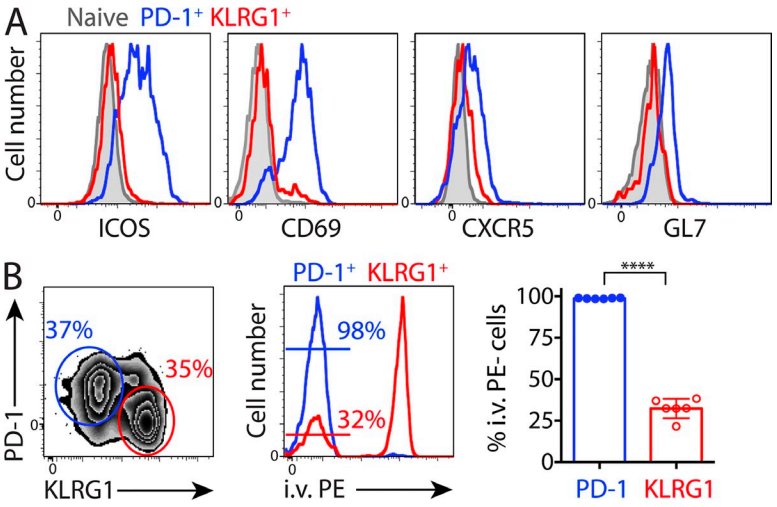

Figure 4. Mtb-specific PD-1+ CD4 T cells express Tfh-associated markers and reside within the lung parenchyma. Mice were infected as described in Fig. 1. (A) Representative flow cytometry histograms show expression of ICOS, CD69, CXCR5, and GL7 by naive CD44^{low} (gray), ESAT-6 tetramer-binding PD-1+KLRG1− (blue), or PD-1−KLRG1+ (red) CD4 T cells recovered from the lungs 60 d after infection. (B) Day 90 after infection, mice were administered i.v. phycoerythrin (PE)-conjugated anti-CD90.2 antibodies 10 min before sacrificing. Representative flow cytometry plot depict gating strategy to identify PD-1+ (blue) and KLRG1+ (red) tetramer-binding CD4 T cells. The flow cytometry histograms show i.v. labeling status of lung tetramer-binding PD-1+ and KLRG1+ CD4 T cells. Numbers in the histogram denotes the percentage of PD-1+ (blue) or KLRG1+ (red) cells that were protected from i.v. PE labeling and are shown for individual mice in the graph on the right. The mean ± SEM for each group is shown; significance was determined by a two-tailed Student's *t* test (****, $P < 0.0001$). Data are representative of three independent experiments with four to five mice per group.

CCR7 and CD127 expression was slightly higher among PD-1+KLRG1− compared with PD-1−KLRG1+ cells, this expression did not approach the levels usually observed on central memory cells that develop when antigen is cleared. In contrast, as we had previously observed for ICOS and CD69 (Fig. 4 A), CXCR3, Ly6C, and CD43 showed markedly distinct expression patterns on these two populations (Fig. 5 A). Most ESAT-6–specific PD-1+KLRG1− cells were CXCR3+, Ly6C−, and CD43+, whereas most PD-1−KLRG1+ cells exhibited the opposite phenotype. In addition, PD-1+KLRG1− cells, like memory cells (Marshall et al., 2011), were intermediate for T-bet expression, whereas PD-1−KLRG1+ cells, like Th1 effector cells, exhibited high T-bet expression (Fig. 3 D). Our results reveal that ESAT-6–specific PD-1+ CD4 T cells, while expressing some markers of effector T cells, also displayed features of memory T cells. In contrast, their KLRG1+ counterparts exhibit characteristics of terminally differentiated effector Th1 cells.

Memory T cells are classically defined as antigen-specific T cells that persist after antigen withdrawal and mount a rapid recall response to subsequent challenge (Sallusto et al., 2010; Bevan, 2011). To address whether PD-1+ cells can survive in the absence of ongoing antigenic stimulation, we sorted (to >95% purity) polyclonal PD-1+KLRG1− and PD-1−KLRG1+ CD4 T cells from the lungs of infected mice and transferred them into congenically marked uninfected mice. Recipient mice were maintained on antibiotics to prevent infection via the transferred cells, and no bacteria were detected in the host spleen, liver, or lung. Although transferred PD-1+ CD4 T cells were maintained at similar numbers throughout the 28 d of the experiment, KLRG1+ cells underwent attrition and by day 8, fivefold fewer cells were recoverable (Fig. 5 B). Despite maintaining their numbers, ∼50% of donor PD-1+ CD4 T cells lost PD-1 expression by day 28. Furthermore, unlike PD-1+ cells transferred into Mtb-infected mice (Reiley et al., 2010), none of the PD-1+ donor cells differentiated into KLRG1+ cells in uninfected recipients, whereas donor KLRG1+ cells maintained their KLRG1+ phenotype (Fig. 5 C). Because ICOS–ICOSL interactions are required to maintain classically defined memory CD4 T cells (Pepper et al., 2011), we also transferred PD-1+ CD4 T cells from Mtb-infected WT mice into ICOSL$^{-/-}$ mice. Interestingly, in preliminary results, in the absence of ICOSL, donor PD-1+ cells underwent attrition similar to that of transferred KLRG1+ cells (Fig. 5 B), and exhibited even lower PD-1 expression (Fig. 5 D). Thus, both antigen and ICOSL signaling contribute to the maintenance of PD-1 expression. ICOSL signaling alone is capable of maintaining overall cell numbers, whereas antigenic stimulation plays a primary role in driving differentiation into KLRG1+ effectors.

Mtb-specific PD-1+ CD4 T cells undergo a robust recall response

To determine whether PD-1+ cells had the capacity to mount a recall response, we challenged mice (with aerosolized Mtb) that had received equal numbers of ESAT-6–specific donor PD-1+KLRG1− or PD-1−KLRG1+ CD4 T cells 10 d before. At 28 d after infection, we found that donor cells derived from PD-1+ precursors had undergone robust expansion, whereas KLRG1+ precursors had not (Fig. 6 A). Furthermore, PD-1+ progenitors had the capacity to differentiate into KLRG1+ cells in response to Mtb challenge. In fact, the profile of PD-1 vs. KLRG1 expression for ESAT-6–specific CD4 T cells derived from transferred PD-1+ cells was nearly identical to that for endogenous tetramer-binding CD4 T cells participating in the primary response to Mtb. Conversely, most of the tetramer-binding cells derived from transferred KLRG1+ cells retained a KLRG1+ phenotype (Fig. 6 B). Overall, despite being subjected to chronic antigenic stimulation and exhibiting some phenotypic markers of effector T cells, lung-resident, Mtb-specific, PD-1+ CD4 T cells share many features with classically defined memory T cells. Like

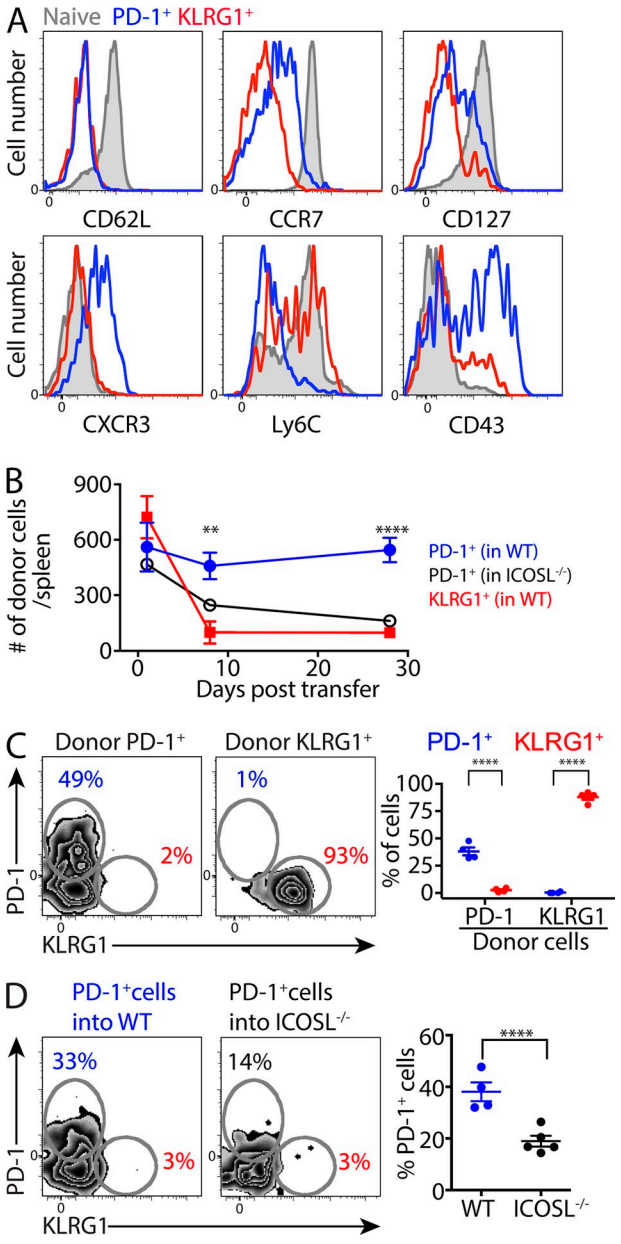

Figure 5. ESAT-6–specific PD-1⁺CD4 T cells express memory associated markers and survive in the absence of antigen via ICOSL signaling. Mice were infected as described in Fig. 1. (A) Representative flow cytometry histograms show expression of the indicated markers by naive CD44^{low} (gray), ESAT-6 tetramer-binding PD-1⁺KLRG1⁻ (blue) or PD-1⁻KLRG1⁺ (red) CD4 T cells (day 120 after infection). (B) PD-1⁺KLRG1⁻ or PD-1⁻KLRG1⁺ CD4 T cells sorted from lungs of Mtb-infected mice (day 119 after infection) were adoptively transferred (10^5 cells/recipient) into uninfected WT or ICOSL$^{-/-}$ mice. The graph shows the number of donor cells recovered from the spleens of WT recipients of donor PD-1⁺ cells (blue), WT recipients of donor KLRG1⁺ cells (red), and ICOSL$^{-/-}$ recipients of donor PD-1⁺ cells (black) at days 1, 8, and 28 after transfer. (C) Flow cytometry plots denote PD-1 and KLRG1 expression by donor-derived (transferred as PD-1⁺KLRG1⁻ or PD-1⁻KLRG1⁺ cells) CD4 T cells in the spleens of WT recipients (28 d after transfer) as described in B. The graph depicts the frequency of cells within each donor-derived population expressing PD-1 (blue) or KLRG1 (red) in individual mice. (D) Flow cytometry plots denote PD-1 and KLRG1 expression by donor-derived PD-1⁺KLRG1⁻ cells in the spleens of WT or ICOSL$^{-/-}$ recipients (28 d after transfer). The graph below depicts the frequency of PD-1⁺ cells within the donor-derived CD4 T cell population in individual mice of each group. The mean ± SEM are shown for each group and statistical significance was determined by a two-tailed Student's *t* test (**, $P < 0.01$; ****, $P < 0.0001$). Data in A are representative of three independent experiments with four to five mice per group. Transfer of PD-1⁺ and KLRG1⁺ cells into WT mice was performed twice with three to five mice per group and per time point whereas transfer of PD-1⁺ cells into ICOSL$^{-/-}$ mice was done once with four to five mice in each of the three time points.

memory T cells, they can persist in the absence of antigen and mount a robust recall response that generates a heterogeneous population of cells resembling the cells responding to a primary infection (Marshall et al., 2011; Pepper et al., 2011; Hale et al., 2013).

Mtb-specific PD-1⁺ CD4 T cells confer greater protection than KLRG1⁺ cells

To directly evaluate the relative capacity of PD-1⁺KLRG1⁻ or PD-1⁻KLRG1⁺ CD4 T cells to provide protection against TB, equivalent numbers (~7×10^5) of each subset isolated from the lungs of donor mice infected with Mtb 80 d before were intravenously transferred into T cell–deficient (TCRβ$^{-/-}$δ$^{-/-}$) recipients 7 d after low-dose aerosolized Mtb infection. Because ESAT-6–specific cells were almost three times more abundant in KLRG1⁺ than in PD-1⁺ donor cells (Fig. 7 A), mice inoculated with PD-1⁺ cells received ~58,000 ESAT-6–specific T cells, whereas those inoculated with KLRG1⁺ cells received ~173,000. When analyzed 28 d after infection (21 d after transfer), most T cells (including ESAT-6–specific T cells) in both experimental groups were found in the lung parenchyma (Fig. 7 B). Consistent with the previous finding that PD-1⁺ T cells exhibit superior survival after transfer into Mtb-infected recipients (Reiley et al., 2010), recipients of PD-1⁺ cells had threefold higher numbers of lung T cells than those receiving KLRG1⁺ cells (Fig. 7 C). Likewise, each group had similar numbers of ESAT-6–specific T cells, despite the fact that recipients of KLRG1⁺ cells initially received three times the number of tetramer-binding cells (Fig. 7 C). Importantly, despite containing only modestly increased numbers of total CD4 T cells and similar numbers of ESAT-6–specific CD4 T cells, recipients of PD-1⁺ cells had dramatically lower bacterial burdens (20-fold vs. 2-fold lower lung CFUs compared with controls) than mice receiving KLRG1⁺ cells (Fig. 7 D). These results provide direct support for the superior protection provided by PD-1⁺ CD4 T cells relative to their KLRG1⁺ counterparts.

Intrinsic ICOS expression is required to maintain ESAT-6–specific CD4 T cells during chronic infection

Given the apparent importance of Mtb-specific PD-1⁺ cells for protective immunity against TB, we next investigated whether expression of molecules typically associated with Tfh

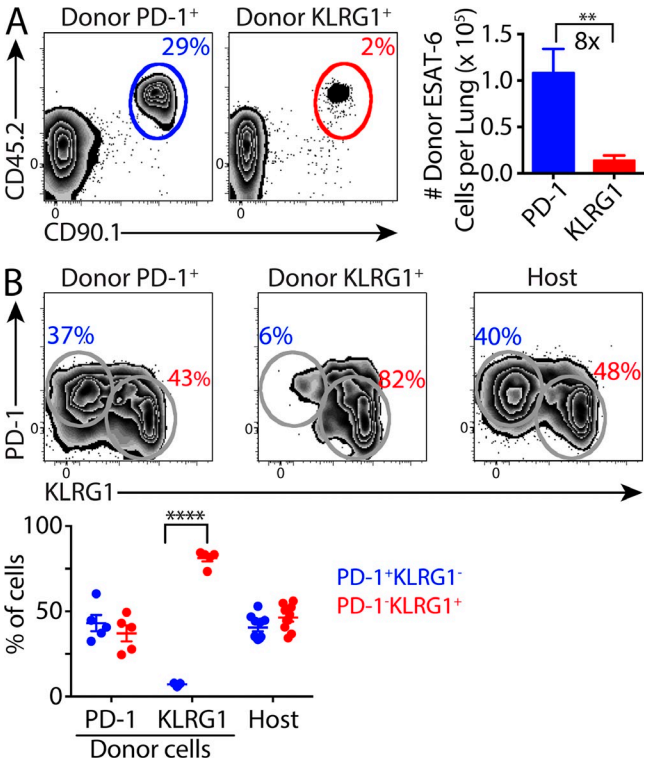

Figure 6. ESAT-6–specific PD-1⁺ CD4 T cells undergo a robust recall response. Mice were infected as described in Fig. 1. 5 mo after infection, PD-1⁺KLRG1⁻ or PD-1⁻KLRG1⁺ CD4 T cells were purified by FACS from lungs of congenically marked donor mice and adoptively transferred (normalized for transfer of 5.5 × 10^4 ESAT-6 tetramer-binding cells/recipient) into uninfected WT mice. Recipients were challenged 10 d after transfer with Mtb and assessed 28 d after infection. (A) Flow cytometry plots depict the percentage of donor-derived cells (CD45.2⁺CD90.1⁺) within the ESAT-6 tetramer-binding CD4 T cell population in recipients receiving either PD-1⁺KLRG1⁻ (left panel) or PD-1⁻KLRG1⁺ (right panel) cells. The bar graph shows the absolute number of donor-derived ESAT-6 tetramer-binding CD4 T cells in the lungs of mice that received PD-1⁺KLRG1⁻ (blue) and PD-1⁻KLRG1⁺ (red) donor cells. (B) Flow cytometry plots depict PD-1 and KLRG1 expression by donor-derived (transferred as PD-1⁺KLRG1⁻ or PD-1⁻KLRG1⁺ cells) and endogenous ESAT-6 tetramer-binding CD4 T cells in recipient lungs. The graph depicts the frequency of PD-1⁺KLRG1⁻ (blue) or PD-1⁻KLRG1⁺ (red) cells within each donor-derived and endogenous ESAT-6 tetramer-binding population in individual mice. The mean ± SEM are shown for each group. Statistical significance was determined by two-tailed Student's *t* test. **, $P < 0.01$; ****, $P < 0.0001$. Data are representative of two independent experiments with five mice per group.

cells was important for the generation or maintenance of the CD4 T cell response. Our data demonstrate that ICOS–ICOSL signals are required to maintain Mtb-specific PD-1⁺ cells in uninfected hosts (Fig. 5). To determine whether ICOS–ICOSL interactions were required to maintain Mtb-specific CD4 T cells in the presence of ongoing antigenic stimulation, we reconstituted sublethally irradiated TCR $\beta^{-/-}\delta^{-/-}$ mice with a 1:1 ratio of WT and ICOS$^{-/-}$ bone marrow. After immune reconstitution, the chimeric mice were infected with Mtb and the ratio of WT to ICOS$^{-/-}$ ESAT-6–specific CD4 T cells in the lungs was evaluated over time. Immediately before infection, chimeric mice had a 1:1 ratio of WT to ICOS$^{-/-}$ CD4 T cells in their blood, and this ratio did not change for naive CD4 T cells isolated from the lungs of infected mice up to ∼180 d after infection (Fig. 8 A). Interestingly, antigen-specific ICOS$^{-/-}$ CD4 T cells had an early competitive advantage over WT cells; at the peak of the T cell response (∼28 d after infection) twice as many ICOS$^{-/-}$ as WT ESAT-6–specific CD4 T cells were recovered from the lungs. However, ICOS$^{-/-}$ CD4 T cells were compromised in their persistence during the chronic stages of infection. The ratio of ICOS$^{-/-}$ to WT ESAT-6–specific T cells progressively declined to 1:6 by day ∼180 (Fig. 8 B), and was associated with an increased ratio of KLRG1⁺ to PD-1⁺ cells within the ICOS$^{-/-}$ population (Fig. 8 C). Furthermore, PD-1⁺ cells efficiently phosphorylated Akt (Fig. 8 D), which, along with their IL-2 production (Fig. 8 E), was dependent on ICOS signaling. In summary, intrinsic expression of ICOS on Mtb-specific CD4 T cells promoted Akt activation, IL-2 production, and the generation and maintenance of the self-renewing PD-1⁺ population. In the absence of ICOS-mediated signaling, robust expansion of short-lived KLRG1⁺ effectors was initially observed, but the Mtb-specific CD4 T cell response was sustained to a much lower degree during the chronic phase of infection.

Intrinsic Bcl6 expression is required for Mtb-specific CD4 T cell proliferation and function

To investigate the role of Bcl6 (a Tfh-associated transcription factor induced by ICOS–ICOSL signaling; Johnston et al., 2009; Nurieva et al., 2009; Yu et al., 2009; Choi et al., 2011) in the induction and maintenance of the CD4 T cell response during Mtb infection, we generated mixed chimeras by reconstituting lethally irradiated WT (CD45.1) mice with Bcl6$^{-/-}$ (CD45.2) and WT (CD45.1/.2) fetal liver cells. After immune reconstitution, and immediately before infection, chimeric mice had a 1:1 ratio of WT to Bcl6$^{-/-}$ CD4 T cells in their blood (Fig. 9 A). Although this 1:1 ratio was maintained in naive CD44^{low} CD4 T cells in the lungs after Mtb infection (Fig. 9 A), numbers of ESAT-6–specific CD4 T cells were heavily skewed in favor of WT T cells (Fig. 9 B). Bcl6$^{-/-}$ T cells comprised only ∼6% of the tetramer-binding population at day 27 after infection, and <1% by day 44. Although the reduced numbers of ESAT-6–specific Bcl6$^{-/-}$ CD4 T cells could be the result of reduced proliferation and/or survival, this reduction was at least partially reflected by diminished proliferation; a smaller fraction of tetramer-binding Bcl6$^{-/-}$ T cells expressed Ki67 compared with their WT counterparts (Fig. 9 C). In addition to compromised proliferation, ESAT-6–specific CD4 T cells lacking Bcl6 exhibited impaired functional differentiation, as indicated by a smaller percentage of KLRG1⁺ cells (Fig. 9 D), reduced T-bet expression, and diminished IFN-γ production assessed directly ex vivo (Fig. 9 E). Overall, our results show that intrinsic expression of Bcl6 is not only critical for the development of the PD-1⁺ population that exhibits Tfh-like properties,

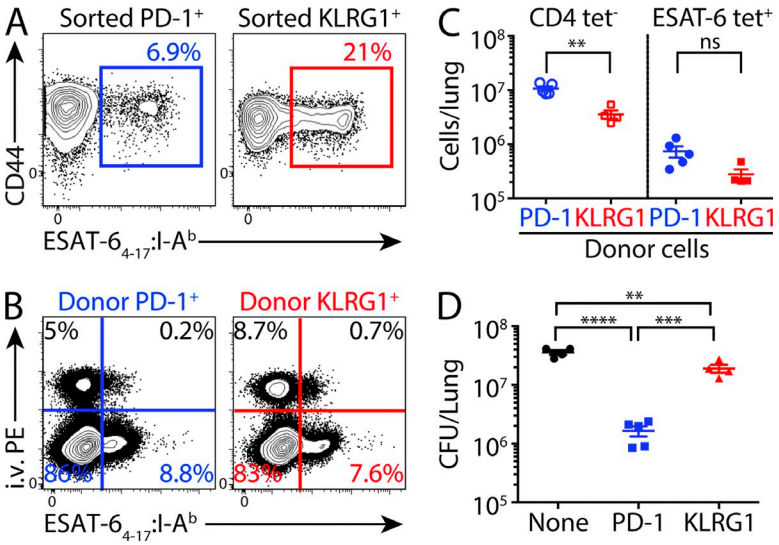

Figure 7. PD-1+ CD4 T cells confer superior protection against Mtb compared with their KLRG1+ counterparts. PD-1+KLRG1− or PD-1−KLRG1+ CD4 T cells were purified by FACS from the lungs of congenically marked Mtb-infected mice (80 d after infection) and transferred into T cell–deficient (TCRβ−/−δ−/−) mice that had been infected with Mtb 7 d prior. Recipients were assessed 28 d after infection (21 d after transfer). (A) Flow cytometry plots depict proportion of ESAT-6 tetramer-binding cells within sorted PD-1+KLRG1− (left) and PD-1−KLRG1+ (right) CD4 T cells before adoptive transfer. (B) Representative flow cytometry plots show ESAT-6 tetramer binding and i.v. PE-antibody labeling for donor-derived CD4 T cells transferred as either PD-1+KLRG1− (left) or PD-1−KLRG1+ (right) cells. (C) Graph shows the number of donor-derived CD4 T cells within the lung parenchyma (i.v. PE−) that either did not (left) or did (right panel) bind the ESAT-6 tetramer in individual recipients after transfer of either PD-1+KLRG1− (blue) or PD-1−KLRG1+ (red) CD4 T cells. (D) Graph depicts lung bacterial burdens in recipients of no T cells (black), PD-1+KLRG1− (blue), or PD-1−KLRG1+ (red) CD4 T cells. The mean ± SEM are shown and statistical significance was determined by two-tailed Student's *t* test (**, P < 0.01; ***, P < 0.001; ****, P < 0.0001). Data are representative of two independent experiments with four to seven mice per group.

but also for the development and function of Mtb-specific effector Th1 cells. These results suggest that during Mtb infection, the vast majority of KLRG1+ effector Th1 cells originate from Bcl-6–dependent PD-1+ precursors.

The chemokine receptor CXCR5 is regulated by Bcl6 (Choi et al., 2011) and intrinsic expression of CXCR5 by CD4 T cells plays an important role in TB immunity (Slight et al., 2013). To address the role of CXCR5 in Mtb-specific CD4 T cells, we generated WT plus CXCR5−/− mixed bone marrow chimeras. Immediately before Mtb infection, reconstituted chimeras showed a 1:1 ratio of WT: CXCR5−/− CD4 T cells in their blood, and this ratio remained at 1:1 for naive T cells isolated from the lung, even at day 119 after infection (Fig. 10 A). In contrast to our findings in Bcl6 chimeras, similar numbers of CXCR5−/− and WT ESAT-6 tetramer-binding CD4 T cells were observed during early infection, but CXCR5−/− cells showed diminished persistence after 120 d after infection (Fig. 10 B). Unlike the phenotypic and functional differences observed in Bcl-6–deficient T cells (Fig. 9); however, CXCR5-deficient and WT T cells showed similar PD-1/KLRG1 profiles, distribution between the lung parenchymal/intravascular compartments, levels of T-bet expression, and direct ex vivo IFN-γ production (unpublished data). Thus, although intrinsic CXCR5 expression is required to maintain Mtb-specific CD4 T cells during chronic infection, the function of CXCR5 only accounts for a small part of the observed function of Bcl6.

DISCUSSION

The frequency of circulating Mtb-specific Th1 cells does not correlate with protection in either human TB or in murine models of TB (Leal et al., 2001; Elias et al., 2005; Fletcher, 2007; Mittrücker et al., 2007; Urdahl et al., 2011; Urdahl, 2014). Recent studies in the murine model demonstrate that Mtb-specific Th1 cells are heterogeneous and include a major population of Th1 progenitor cells that are not fully differentiated, and that express high levels of PD-1, generate low levels of IFN-γ, and reside in the lung parenchyma (Reiley et al., 2010; Sakai et al., 2014). Although prior studies suggested that these progenitor cells are more protective than their terminally differentiated KLRG1+ Th1 counterparts, we directly demonstrated this enhanced protection in adoptive transfer experiments. The emerging importance of PD1+ Th1 progenitor cells in immunity against TB led us to investigate the antigenic and molecular requirements for their induction and survival.

We found that ESAT-6–specific T cells are continuously exposed to Mtb antigen throughout the acute and chronic phases of infection. Thus, the concept that Mtb escapes T cell–mediated immunity by sequestering or reducing expression of its antigenic proteins, as had been previously shown for T cells recognizing Ag85B, a specific antigenic mycobacterial protein (Bold et al., 2011; Egen et al., 2011), does not hold for ESAT-6. Whereas Ag85B is an enzyme involved in Mtb cell wall synthesis and whose expression is drastically reduced during chronic Mtb infection as bacterial replication slows (Rogerson et al., 2006), ESAT-6, an immunodominant antigen in both mice and humans, is a secreted virulence factor that is available for immune recognition during all stages of infection. Which cell-type is responsible for continuous presentation of ESAT-6 antigen is currently unknown, as is whether this cell is directly infected with Mtb or has picked-up Mtb components from infected cells (Srivastava and Ernst, 2014). In confirmation of earlier studies (Reiley et al., 2010), we found that among the ESAT-6–specific population, the major in vivo source of IFN-γ was the KLRG1+ population, whereas PD-1+KLRG1− cells were the principal proliferating population.

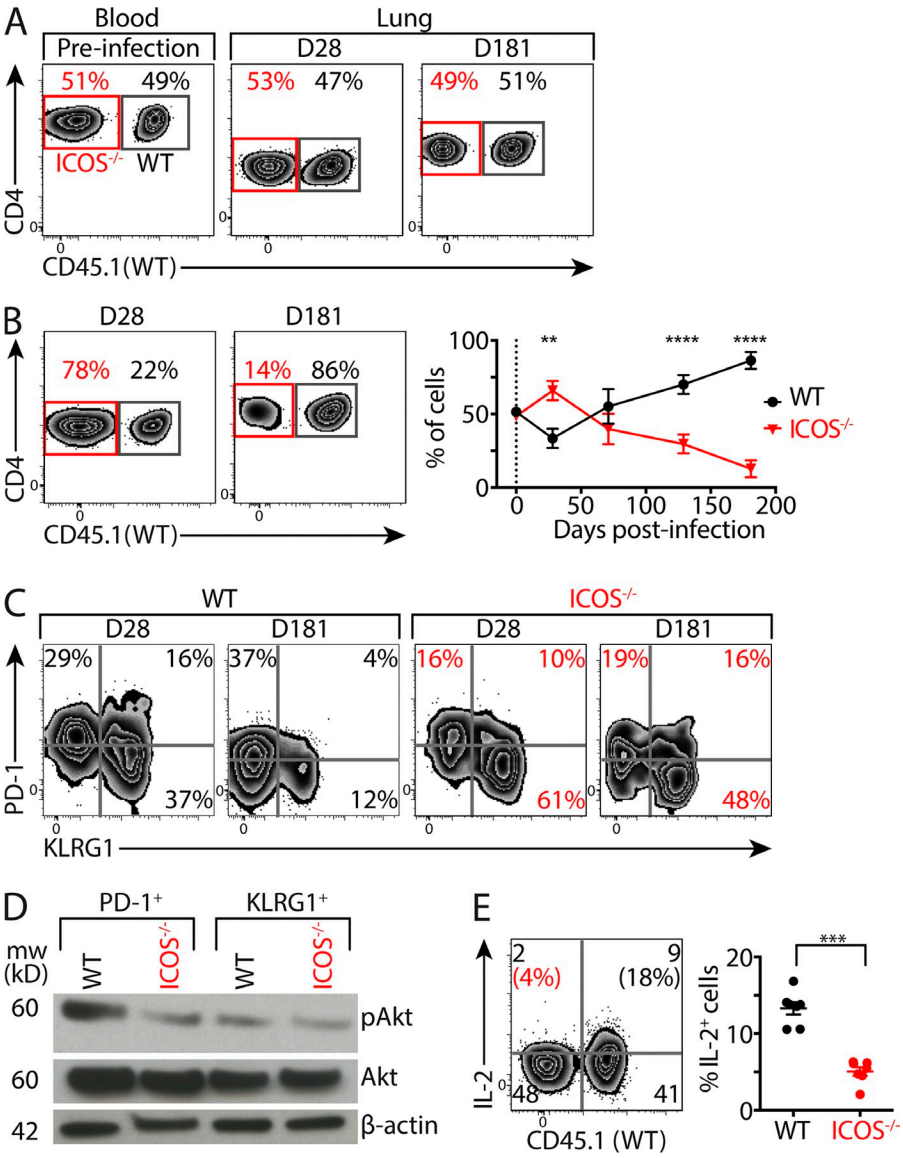

Figure 8. T cell–intrinsic ICOS signaling is required to maintain ESAT-6–specific CD4 T cells. TCRβ$^{-/-}$δ$^{-/-}$ mice were sublethally irradiated (600 rads) and reconstituted with a 1:1 mix of congenically marked WT and ICOS$^{-/-}$ bone marrow cells. 10 wk after reconstitution, the mice were infected with Mtb as described in Fig. 1. (A) Representative flow cytometry plots depict the ratio of WT (black) and ICOS$^{-/-}$ (red) CD4 T cells in blood 10 wk after reconstitution and among naive lung (CD44^{low}) CD4 T cells at days 28 and 181 after infection. (B) Flow cytometry plots and graph show the frequency of WT (black) and ICOS$^{-/-}$ (red) cells within the ESAT-6–specific CD4 T cell population at the indicated time points. (C) Representative flow cytometry plots depict the expression of PD-1 and KLRG1 by WT and ICOS$^{-/-}$ ESAT-6–specific CD4 T cells at the indicated time points. (D) PD-1^{+} or KLRG1^{+} CD4 T cells (WT or ICOS$^{-/-}$) were sorted by FACS from the lungs of chimeric mice (70 d after infection) and analyzed by Western blot for Akt phosphorylation. (E) Single cell suspensions from the lungs of chimeric mice were stimulated with ESAT-6_{4-17} in vitro and intracellular cytokine staining was performed. A representative flow plot depicts CD45.1 (WT cells) and IL-2 expression within CD4 T cells coproducing IFN-γ and TNF (gate not depicted), and numbers in parentheses represent the percentage of WT (black) and ICOS$^{-/-}$ (red) cells within this population that express IL-2. The graph shows this value for each population within individual chimeric mice. The mean ± SEM are shown. Statistical significance was determined by two-tailed Student's *t* test (**, $P < 0.01$; ***, $P < 0.001$; ****, $P < 0.0001$). Data shown in A–C and E are representative of three independent experiments with four to seven mice per group and per time point, and data in D are representative of two independent experiments with cells pooled from four mice.

Despite ongoing antigen-driven proliferation, we found that PD-1^{+}KLRG1^{-} Mtb-specific T cells retain memory-like properties, including survival in the absence of antigen and the ability to mount robust secondary responses and generate Th1 (T-bet^{hi}KLRG1^{+}) effectors. The findings that PD-1–expressing cells undergo robust proliferation, produce polyfunctional cytokines, and mediate superior protection compared with PD-1^{-}KLRG1^{+} cells was initially somewhat surprising because PD-1 was first identified as a marker for functionally exhausted T cells (Barber et al., 2006; Day et al., 2006). PD-1 signaling can restrict T cell activation by inhibiting Akt activation; however, these studies were performed in CD8 T cells that did not express ICOS (Riley, 2009). In our studies, Akt phosphorylation was highest in PD-1^{+} Mtb-specific CD4 T cells, and this activation was dependent on ICOS. These results are consistent with the fact that PD-1 can also mark recently activated T cells, including Tfh cells (Crotty, 2011). Because PD-1–mediated inhibitory signals increase the TCR threshold for antigenic stimulation (Honda et al., 2014), it is tempting to speculate that PD-1 signaling elevates the level of TCR signaling required to drive terminal differentiation. If this were the case, CD4 T cell expression of PD-1 might serve a beneficial role during TB by restricting terminal differentiation, thereby prolonging and preventing an excessive CD4 T cell response. Consistent with this, CD4 T cell expression of PD-1 during TB is host protective; PD-1–deficient mice rapidly succumb to a severe inflammatory form of TB that is driven by a profound expansion of Mtb-specific CD4 T cells (Lázár-Molnar et al., 2010; Barber et al., 2011). However, the precise role of PD-1 in modulating antigen-specific CD4

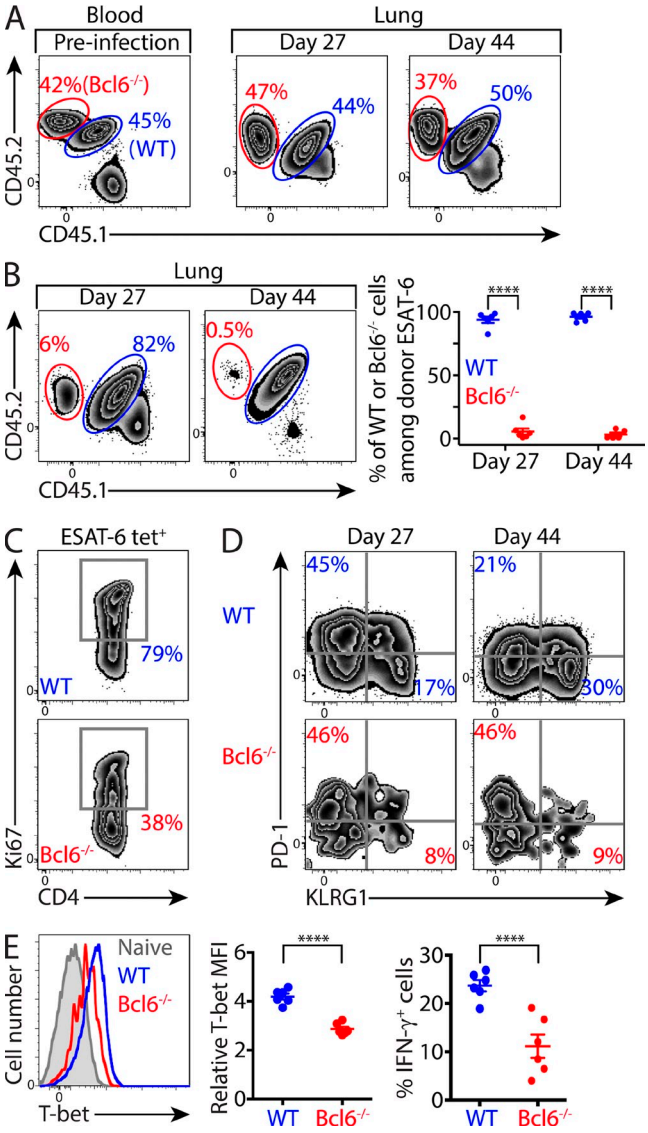

Figure 9. T cell–intrinsic Bcl6 signaling is required to generate an ESAT-6–specific Th1 response. C57BL/6 WT mice were lethally irradiated (1000 Rads) and reconstituted with a 1:1 mix of congenically WT and Bcl6$^{-/-}$ fetal liver cells. 10 wk after reconstitution, mice were infected with Mtb as described in Fig. 1. (A) Representative flow cytometry plots depict the frequency of WT (blue) and Bcl6$^{-/-}$ (red) CD4 T cells in blood 10 wk after immune reconstitution and among naive lung (CD44^{low}) CD4 T cells at days 27 and 44 after infection. (B) Flow cytometry plots depict the frequency of WT (blue) and Bcl6$^{-/-}$ (red) derived cells within the ESAT-6 tetramer-binding CD4 T cell population in the lungs of chimeric mice at the indicated time points. The graph depicts the percentage of WT (blue) and Bcl6$^{-/-}$ (red) cells within the donor-derived ESAT-6 tetramer-binding CD4 T cell populations (excludes host-derived cells). (C) Representative flow cytometry plots depict the percentage of WT or Bcl6$^{-/-}$ ESAT-6 tetramer-binding CD4 T cells that express Ki67 at day 27 after infection. (D) Representative flow cytometry plots show PD-1 and KLRG1 expression by WT or Bcl6$^{-/-}$ ESAT-6 tetramer-binding CD4 T cells at the indicated time points after infection. (E) Representative flow cytometry histograms (left) show T-bet expression by naive CD4 T cells (gray), WT (blue), and Bcl6$^{-/-}$ (red) ESAT-6 tetramer-binding CD4 T cells (27 d after infection). The graph (middle) shows the T-bet MFI for WT and Bcl6$^{-/-}$populations relative to expression in naive CD4 T cells. The graph on the right depicts the percentage of WT and Bcl6$^{-/-}$ lung ESAT-6 tetramer-binding CD4 T cells producing IFN-γ directly ex vivo (27 d after infection). The mean ± SEM are shown. Statistical significance was determined by two-tailed Student's *t* test (****, $P < 0.0001$). Data are representative of two independent experiments with 3–7 mice per group at each time point.

T cell expansion and differentiation during TB remains unclear and needs to be further investigated.

Although PD-1^{+}KLRG1^{-} T cells resident in the Mtb-infected lung parenchyma exhibited many Tfh-like properties, Tfh cells are usually found within lymphoid follicles or circulating in the blood (Crotty, 2011). Mtb infection may trigger ectopic lymphangiogenesis within infected lungs, resulting in granulomatous inflammation with B and T cell containing follicular structures whose formation is dependent on CXCL13 and CXCR5 (Kahnert et al., 2007; Khader et al., 2009; Slight et al., 2013). We found that ICOS, Bcl6, and CXCR5 are not only markers of Tfh-like cells, but that each of these molecules contributes to the maintenance of Mtb-specific CD4 T cells during chronic infection, albeit to varying degrees. Although ICOS, Bcl6, and CXCR5 are part of the same pathway in Tfh development (ICOS induces Bcl6, which in turn induces CXCR5; Choi et al., 2011), it is not clear how other pathways may intersect with this regulation during the inflammatory milieu of TB. Our findings indicate that the relationship between these molecules during TB is not strictly linear, as Bcl6 expression alone could not explain the phenotype associated with ICOS deficiency, nor was CXCR5 responsible for the severely impaired Th1 development associated with Bcl6 deficiency. Overall, however, our results suggest that interactions within the follicular structures of granulomas are critical for maintaining the pulmonary Th1 response during chronic infection.

CXCR5^{+} CD4 T cells are critical for protective immunity against Mtb (Slight et al., 2013); CXCR5$^{-/-}$ mice are susceptible to TB, and this heightened susceptibility can be completely reversed by providing CD4 T cells from CXCR5-sufficient mice. One possible explanation for these results is that CXCR5^{+} CD4 T cells mediate immunity by localizing CD4 effectors to Mtb-infected cells. Our finding that CXCR5 expression by CD4 T cells contributes to the maintenance of Th1 cells during chronic infection suggests an additional possibility: CXCR5 may direct CD4 T cells to follicular sites where they receive signals for their survival and differentiation into effector cells with mycobacteriocidal properties. These possibilities are not mutually exclusive and each warrants further investigation.

As for classically defined memory CD4 T cells, maintenance of Mtb-specific progenitors was found to depend on ICOS–ICOSL signaling both during ongoing infection and after transfer to uninfected mice. Surprisingly, ICOS$^{-/-}$ CD4 T cells had a competitive advantage over WT CD4 T cells in mixed chimeras during early Mtb infection, but later suffered accelerated attrition. These outcomes could be explained by the

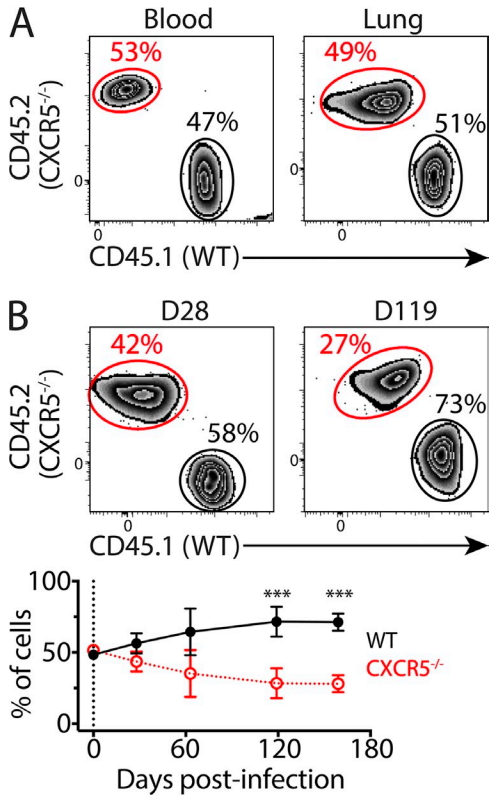

Figure 10. CXCR5 is required in a cell-intrinsic manner to maintain ESAT-6–specific CD4 T cells during chronic Mtb infection. TCRβ$^{-/-}$δ$^{-/-}$ mice were sublethally irradiated (600 rads) and reconstituted with a 1:1 mix of congenically marked WT and CXCR5$^{-/-}$ bone marrow cells. Mice were infected as described in Fig. 1 at 10 wk after reconstitution. (A) Representative flow cytometry plots denote the frequency of WT (black) and CXCR5$^{-/-}$ (red) CD4 T cells in blood 10 wk after bone marrow reconstitution (left) and among naive lung CD4 T cells at 119 d after infection. (B) Representative flow cytometry plots and graph shows the frequency of WT (black) and CXCR5$^{-/-}$ (red) ESAT-6 tetramer-binding CD4 T cells within the lung at the indicated time points. The mean ± SEM are shown. Significance was determined by two-tailed Student's *t* test (**, $P < 0.001$). Data are representative of three independent experiments with three to seven mice per group at time point.

reduced expression by ICOS$^{-/-}$ cells of PD-1 and their more rapid progression into terminally differentiated KLRG1^{+} Th1 cells. ICOS signaling (together with TCR signaling) promotes PD-1 expression in Mtb-specific CD4 T cells. Collectively, these findings support the idea that PD-1 may function to restrict CD4 T cell expansion and terminal differentiation, which may ultimately serve to maintain the Th1 response during chronic infection. Interestingly, and in contrast to the importance of B cells in the maintenance of memory CD4 T cells after acute infections (Pepper et al., 2011; Mollo et al., 2013), Mtb-infected μMT$^{-/-}$ mice lacking B cells had normal numbers of ESAT-6–specific CD4 T cells throughout infection (unpublished data). This likely reflects the fact that B cells are the primary cell type expressing ICOSL in uninfected animals after antigen clearance (Pepper et al., 2011), whereas ICOSL is expressed by multiple myeloid populations, including dendritic cells, in Mtb-infected mice (unpublished data).

In contrast to ICOS deficiency, Bcl6 deficiency had a dramatic impact on the induction of the Mtb-specific CD4 T cell response, with very few Bcl6$^{-/-}$ cells found among the ESAT-6–specific T cell pool at the peak of the immune response. Furthermore, the few Bcl6$^{-/-}$ Mtb-specific CD4 T cells induced were impaired in their function. These results are consistent with findings from recent studies showing that optimal Th1 polarization upon in vitro stimulation requires collaboration between T-bet and Bcl6 (Nakayamada et al., 2011; Oestreich et al., 2011, 2012). However, to our knowledge, this is the first study to show that Bcl6 is critical for induction of a Th1 effector response in vivo. In fact, during acute *Listeria* infection, Bcl6$^{-/-}$ CD4 T cells showed normal differentiation into Th1 effectors, despite an impaired memory response (Pepper et al., 2011). A potential explanation for this difference is that effector T cells may arise directly from naive precursors during acute *Listeria* infection, but develop from a Bcl6-dependent progenitor population during chronic Mtb infection.

Our findings provide a framework for understanding how the CD4 T cell response is maintained in the Mtb-infected lung. Molecular pathways associated with lymphatic follicles (those dependent on ICOS and Bcl6) and a chemokine receptor (CXCR5) associated with trafficking to lymphatic follicles are critical in sustaining the Th1 response, even during ongoing antigenic stimulation. This understanding may provide new avenues to facilitate the induction and maintenance of the Th1 progenitor populations that mediate durable protection against TB.

MATERIALS AND METHODS

Mice. C57BL/6 (B6), C57BL/6.PL (B6.PL, CD90.1), B6.SJL-Ptprc^{a}-Pep3^{b}BoyJ (B6.SJL, CD45.1), B6.129S2 (Cg)-Blr1^{tm1Ijpp}/J (CXCR5$^{-/-}$), B6.129P2-ICOS^{tm1Mak}/J (ICOS$^{-/-}$), B10.129S2 (B6)-Igh-6^{tm1Cgn}/J (μMT$^{-/-}$), B6.129P2-Icosl^{tm1mak}/J (ICOSL$^{-/-}$), B6.Cg-Tg(TcraTcrb)425Cbn/J (OT-II), and B6.129P2-Tcrb^{tm1Mom}Tcrd^{tm1Mom}/J (TCRβ$^{-/-}$δ$^{-/-}$) were purchased from The Jackson Laboratory. Heterozygous mice deficient in one allele of the Bcl6 gene (Bcl6$^{+/-}$) were maintained on a B6 background and have been described previously (Dent et al., 1997). ESAT-6 TCRtg (C7) mice were provided by E. Pamer (Memorial Sloan Kettering Cancer Center, New York, NY) and have been described previously (Gallegos et al., 2008). All mice were housed and bred under specific pathogen–free conditions at Seattle Biomedical Research Institute (SBRI) and the University of Washington. The Institutional Animal Care and Use Committee of SBRI and or the University of Washington approved all experimental protocols involving animals.

Generation of mixed lymphocyte chimeric mice. To generate mixed bone marrow chimeras, bone marrow cells from congenically marked WT, ICOS$^{-/-}$, or CXCR5$^{-/-}$ mice were isolated. Mature B and T cells were depleted from the bone marrow cell preparation by adding biotinylated anti–mouse CD19 to a mouse CD3ε micro-bead kit (Miltenyi Biotec). Congenically marked WT and knockout (ICOS$^{-/-}$ or CXCR5$^{-/-}$) cells were mixed in a ratio of 1:1 and co-injected (1–5 × 10^{6} of each) into sublethally irradiated (600 rads from a Rad Source gamma irradiator) T cell–deficient (TCRβ$^{-/-}$δ$^{-/-}$) mice. As Bcl6 deficiency on a B6 background is embryonic lethal (Yu et al., 2009; Higdon et al., 2014), we used a mixed fetal liver chimera approach. For this, timed pregnancies from congenically marked WT (CD45.1 and CD45.2) pairs and Bcl6 heterozygous pairs (CD45.2)

were established. At embryonic day 15.5 or 16.5, pregnant mice were sacrificed and fetuses collected. Fetal livers were isolated and teased into single cell suspension. Tail snips of the fetuses were screened for Bcl6 deficiency by PCR (Higdon et al., 2014). Typed $Bcl6^{-/-}$ and WT fetal liver cells were then mixed at a ratio of 1:1 and co-injected (2×10^6 of each) into lethally irradiated (1,000 Rad) congenically marked B6.SJL mice. All recipient mice were put on prophylactic antibiotics for 4 wk and their blood was screened for immune reconstitution 8–10 wk after bone marrow or fetal liver cell transfer, followed by infection with Mtb.

Aerosol infections and bacterial load determination. Infection with a stock of Mtb H37Rv was done as previously described (Urdahl et al., 2003). In brief a stock of Mtb was sonicated before use and mice were infected in an aerosol infection chamber (Glas-Col) with ∼100 CFU deposited in the lungs of each mouse. Two mice were sacrificed immediately after infection to determine the infectious dose for each experiment. To determine viable numbers of CFUs, the left lung of each mouse was homogenized in 0.05% Tween 80 in PBS. 10-fold serial dilutions were made in 0.05% Tween 80 and plated on 7H10 plates. Colonies were counted after 21 d of incubation at 37°C to determine CFUs per organ.

In vivo intravascular labeling of T cells. Intravascular T cells were labeled in vivo by intravenous injection of 1 µg PE-conjugated antibodies against T cell markers (CD90.2) 5–10 min before sacrifice (Anderson et al., 2014; Sakai et al., 2014). In some experiments in vivo labeling was done by antibodies against the CD4 molecule (clone RM4-4; eBioscience) followed by ex vivo staining for the CD4 marker using a noncrossblocking antibody (RM4-5; Invitrogen).

Preparation of single-cell suspensions. Lungs were perfused with 5 ml of PBS via injection through the right ventricle. The perfused lungs were harvested into Hepes buffer containing liberase blendzyme 3 (Roche) and DNase (Sigma-Aldrich). The lungs were then minced into small pieces using the gentleMacs dissociator (Miltenyi Biotec) and incubated at 37°C for 30 min, followed by homogenization with the gentleMacs dissociator. The single-cell suspensions were then filtered using a cell strainer. Single-cell suspensions of the spleens and lung draining lymph nodes (pLNs) were made by crushing the tissues between two glass slides. The cells were filtered using cell strainers and suspended in FACs buffer (PBS containing 2.5% fetal bovine serum and 0.1% NaN_3). For adoptive transfer, NaN_3 was excluded from the FACs buffer. In experiments involving intracellular cytokine detection, incubation steps were performed in media/buffers containing Brefeldin A (10 µg/ml; Sigma-Aldrich). For CXCR5 staining, lung cells were isolated using the enzyme-free cell dissociation buffer (Invitrogen).

Cell enrichment, sorting and adoptive transfer. For adoptive transfer experiments, CD4 T cells were negatively enriched to >95% purity from fleshly isolated spleens, pLNs and/or lungs using Miltenyi Biotec magnetic microbeads and subsequent column purification according to the manufacturer's protocol. In some cases the negatively enriched cells were stained with anti-mouse PD-1 and anti-mouse KLRG1 antibodies (BioLegend) and sorted on a cell sorter (FACSAria; BD Bioscience). The enriched or sorted cells were transferred with or without CFSE labeling into naive or infected mice. For recall experiments, polyclonal CD4 T cells expressing PD-1 or KLRG1 were sorted from donor B6.PL (CD45.2 x CD90.1) mice 120 d after infection with Mtb and adoptively transferred (10^5 cells) into naive B6.SJL mice. Recipient mice were rested for 10 d, challenged with low dose aerosol Mtb, and sacrificed 28 d later. For some experiments adoptively transferred cells were labeled with CFSE using the CellTrace CFSE cell proliferation kit following the manufactures protocol (Life Technologies). In brief, single-cell suspensions were incubated dilute CFSE at a final concentration of 5 µM for 10 min before quenching with complete growth medium with 10% fetal bovine serum.

For protection experiments, polyclonal PD-1^+ and KLG1^+ cells were sorted from WT B6 mice 80 d after Mtb infection. Approximately 7×10^5 CD4 T cells of each subset (which translated to ∼58,000 ESAT-6–specific PD-1^+ cells and ∼173,000 ESAT-6–specific KLRG1^+ cells) were adoptively transferred into T cell–deficient (TCR$\beta^{-/-}\delta^{-/-}$) mice infected with Mtb 7 d before. Recipient mice were sacrificed 28 d after infection and analyzed for the expansion of donor cells and lung bacterial burdens.

Detection of Mtb-specific CD4 T cells. MHCII tetramers containing amino acids 4–17 of Mtb ESAT-6 were used to detect Mtb-specific CD4 T cells. *Drosophila* S2 cells transfected with pRMHa-3 vector containing the sequence for the stimulatory residues of ESAT-6 protein (QQWNFAGIEAAASA) of Mtb was a gift from M. Jenkins (University of Minnesota, Minneapolis, MN). Production of the peptide:I-A^b monomeric molecules, and tetramerization of biotinylated peptide:I-A^b with phycoerythrin (PE) or allophycocyanin (APC) fluorophores (Prozyme), was performed as previously described (Moon et al., 2007). In addition, APC-conjugated tetramers (ESAT-$6_{4–17}$:I-A^b) were obtained from the National Institutes of Health Tetramer Core Facility. Single-cell lymphocyte preparations were stained at saturating concentrations with the tetramers and incubated at room temperature for 1 h.

Cell surface staining. Fc receptors were blocked with purified anti–mouse CD16/32 (2.4G2; BD). The cells were suspended in FACS buffer and stained at saturating conditions with the anti–mouse monoclonal antibodies against CD3 (145-2C11; eBioscience), CD4 (RM4-5; Invitrogen), CD44 (1M7; eBioscience), CD8 (53–6.7; eBioscience), PD-1 (RMP1-30; BioLegend), KLRG1 (2F1; BioLegend), Ly6C (HK1.4; eBioscience), CD62L (MEL-14; eBioscience), CD127 (A7R34; eBioscience), and CD43 (S7; BD). To exclude cells that may have nonspecifically bound to the tetramers, antibodies against non–T cell markers F4/80 (BM8; eBioscience), CD19 (eBio1D3; eBioscience), CD11c (N418; eBioscience), and CD11b (M1/70; eBioscience) were included in a dump channel. All surface staining was done at 4°C for 30 min, except staining for CXCR3 (CXCR3-173; eBioscience), CXCR5 (2G8; BD), and CCR7 (4B12; eBioscience), which was done at room temperature for 1 h. Samples were fixed in PBS containing 2% paraformaldehyde.

Intracellular cytokine and transcription factor staining. After tetramer and or surface staining, the cells were fixed, permeabilized, and stained with antibodies against intracellular markers using eBioscience fixation/permeabilization and permeabilization buffers. For detection of inducible IFN-γ, TNF, and IL-2, lung single-cell suspensions were stimulated in vitro with $ESAT_{4–17}$ peptide (5 µg/ml final concentration) or anti-CD3ε (145-2C11; BD) and CD28 (37.51; BD) at a final concentration of 0.03 µg/ml anti-CD3ε and 0.5 µg/ml anti-CD28. The cells were subsequently cultured for 4 h in complete growth medium (RPMI 1640 supplemented with 10% FCS, 2 mM L-glutamine, 10 mM HEPES, 0.5 µM 2-ME, 100 U/ml penicillin, and 100 µg/ml streptomycin). Cells were washed, stained with antibodies against surface markers, permeabilized, and fixed as described above. The cells were then stained using anti–mouse IFN-γ (XMG1.2, BD), anti–mouse IL-2 (JES6-5H4; BioLegend), anti–mouse TNF (MP6-XT22; eBioscience), anti–mouse Ki67 (SolA15; eBioscience), anti–mouse T-bet (4B10; BioLegend), and anti–mouse Bcl6 (K112-91; BD). The cells were incubated at 4°C for 30 min, washed, resuspended in PBS, and analyzed by flow cytometry. In some experiments, mice were injected with Cyclosporin A (R&D Systems) intraperitoneally 4 h before harvest of mice for detection of direct ex vivo IFN-γ. Cyclosporin A was diluted in olive oil and mice were injected with a 200-µl vol, at a dose of 25 mg/kg body weight.

Western blot analysis. CD4 T cells were purified by negative enrichment from WT and $ICOS^{-/-}$ mixed bone marrow chimeric mice. The cells were then stained with anti-mouse PD-1, KLRG1 and the congenic markers for WT and $ICOS^{-/-}$ cells. PD-$1^+$and KLRG1^+ cells of WT or $ICOS^{-/-}$ origin were sorted and lysed for protein analysis by Western blotting following standard techniques. In brief, nitrocellulose membranes were probed with rabbit anti-phospho-Akt and rabbit anti–pan-Akt (Cell Signaling Technology) or rabbit anti–mouse β-actin1-HRP antibody (Jackson ImmunoResearch Laboratories). A secondary rat anti–rabbit-HRP antibody (Jackson ImmunoResearch Laboratories) was used to detect the primary antibodies.

Data acquisition and analysis. Data from stained cells were acquired using the BD LSRII flow cytometer. Flow data were analyzed using FlowJo software (Tree Star). Statistical analysis and graphical representation of data were done using GraphPad Prism software. Statistical significance was determined by Student's *t* test and denoted as *, $P \leq 0.05$; **, $P \leq 0.001$; ***, $P \leq 0.001$; and ****, $P \leq 0.0001$.

We thank K. Adams, M. Pepper, C. Plumlee, and W. Reiley for comments on the manuscript.

This work was funded by grants to K.B.U. from the National Institutes of Health (U19 AI106761 and R01 AI076327) and from the Paul G. Allen Family Foundation and to P.J.F. from the National Institutes of Health (R21 AI097950 and R01 AI064318). A.O.M was supported by an award from the National Institutes of Health (T21-CA009537) and by a Bank of America Dissertation Fellowship.

The authors declare no competing financial interests.

Submitted: 8 August 2014
Accepted: 18 February 2015

REFERENCES

Andersen, P., and J.S. Woodworth. 2014. Tuberculosis vaccines—rethinking the current paradigm. *Trends Immunol.* 35:387–395. http://dx.doi.org/10.1016/j.it.2014.04.006

Anderson, K.G., K. Mayer-Barber, H. Sung, L. Beura, B.R. James, J.J. Taylor, L. Qunaj, T.S. Griffith, V. Vezys, D.L. Barber, and D. Masopust. 2014. Intravascular staining for discrimination of vascular and tissue leukocytes. *Nat. Protoc.* 9:209–222. http://dx.doi.org/10.1038/nprot.2014.005

Barber, D.L., E.J. Wherry, D. Masopust, B. Zhu, J.P. Allison, A.H. Sharpe, G.J. Freeman, and R. Ahmed. 2006. Restoring function in exhausted CD8 T cells during chronic viral infection. *Nature.* 439:682–687. http://dx.doi.org/10.1038/nature04444

Barber, D.L., K.D. Mayer-Barber, C.G. Feng, A.H. Sharpe, and A. Sher. 2011. CD4 T cells promote rather than control tuberculosis in the absence of PD-1-mediated inhibition. *J. Immunol.* 186:1598–1607. http://dx.doi.org/10.4049/jimmunol.1003304

Barnden, M.J., J. Allison, W.R. Heath, and F.R. Carbone. 1998. Defective TCR expression in transgenic mice constructed using cDNA-based alpha- and beta-chain genes under the control of heterologous regulatory elements. *Immunol. Cell Biol.* 76:34–40. http://dx.doi.org/10.1046/j.1440-1711.1998.00709.x

Bevan, M.J. 2011. Understand memory, design better vaccines. *Nat. Immunol.* 12:463–465. http://dx.doi.org/10.1038/ni.2041

Bold, T.D., N. Banaei, A.J. Wolf, and J.D. Ernst. 2011. Suboptimal activation of antigen-specific CD4+ effector cells enables persistence of M. tuberculosis in vivo. *PLoS Pathog.* 7:e1002063. http://dx.doi.org/10.1371/journal.ppat.1002063

Choi, Y.S., R. Kageyama, D. Eto, T.C. Escobar, R.J. Johnston, L. Monticelli, C. Lao, and S. Crotty. 2011. ICOS receptor instructs T follicular helper cell versus effector cell differentiation via induction of the transcriptional repressor Bcl6. *Immunity.* 34:932–946. http://dx.doi.org/10.1016/j.immuni.2011.03.023

Cooper, A.M. 2009. Cell-mediated immune responses in tuberculosis. *Annu. Rev. Immunol.* 27:393–422. http://dx.doi.org/10.1146/annurev.immunol.021908.132703

Crotty, S. 2011. Follicular helper CD4 T cells (TFH). *Annu. Rev. Immunol.* 29:621–663. http://dx.doi.org/10.1146/annurev-immunol-031210-101400

Day, C.L., D.E. Kaufmann, P. Kiepiela, J.A. Brown, E.S. Moodley, S. Reddy, E.W. Mackey, J.D. Miller, A.J. Leslie, C. DePierres, et al. 2006. PD-1 expression on HIV-specific T cells is associated with T-cell exhaustion and disease progression. *Nature.* 443:350–354. http://dx.doi.org/10.1038/nature05115

Deffur, A., N.J. Mulder, and R.J. Wilkinson. 2013. Co-infection with *Mycobacterium tuberculosis* and human immunodeficiency virus: an overview and motivation for systems approaches. *Pathog Dis.* 69:101–113. http://dx.doi.org/10.1111/2049-632X.12060

Dent, A.L., A.L. Shaffer, X. Yu, D. Allman, and L.M. Staudt. 1997. Control of inflammation, cytokine expression, and germinal center formation by BCL-6. *Science.* 276:589–592. http://dx.doi.org/10.1126/science.276.5312.589

Egen, J.G., A.G. Rothfuchs, C.G. Feng, M.A. Horwitz, A. Sher, and R.N. Germain. 2011. Intravital imaging reveals limited antigen presentation and T cell effector function in mycobacterial granulomas. *Immunity.* 34:807–819. http://dx.doi.org/10.1016/j.immuni.2011.03.022

Elias, D., H. Akuffo, and S. Britton. 2005. PPD induced in vitro interferon gamma production is not a reliable correlate of protection against Mycobacterium tuberculosis. *Trans. R. Soc. Trop. Med. Hyg.* 99:363–368. http://dx.doi.org/10.1016/j.trstmh.2004.08.006

Fletcher, H.A. 2007. Correlates of immune protection from tuberculosis. *Curr. Mol. Med.* 7:319–325. http://dx.doi.org/10.2174/156652407780598520

Fortin, A., L. Abel, J.L. Casanova, and P. Gros. 2007. Host genetics of mycobacterial diseases in mice and men: forward genetic studies of BCG-osis and tuberculosis. *Annu. Rev. Genomics Hum. Genet.* 8:163–192. http://dx.doi.org/10.1146/annurev.genom.8.080706.092315

Gallegos, A.M., E.G. Pamer, and M.S. Glickman. 2008. Delayed protection by ESAT-6-specific effector CD4+ T cells after airborne M. tuberculosis infection. *J. Exp. Med.* 205:2359–2368. http://dx.doi.org/10.1084/jem.20080353

Gallegos, A.M., J.W. van Heijst, M. Samstein, X. Su, E.G. Pamer, and M.S. Glickman. 2011. A gamma interferon independent mechanism of CD4 T cell mediated control of M. tuberculosis infection in vivo. *PLoS Pathog.* 7:e1002052. http://dx.doi.org/10.1371/journal.ppat.1002052

Hale, J.S., B. Youngblood, D.R. Latner, A.U. Mohammed, L. Ye, R.S. Akondy, T. Wu, S.S. Iyer, and R. Ahmed. 2013. Distinct memory CD4+ T cells with commitment to T follicular helper- and T helper 1-cell lineages are generated after acute viral infection. *Immunity.* 38:805–817. http://dx.doi.org/10.1016/j.immuni.2013.02.020

Higdon, L.E., K.A. Deets, T.J. Friesen, K.Y. Sze, and P.J. Fink. 2014. Receptor revision in CD4 T cells is influenced by follicular helper T cell formation and germinal-center interactions. *Proc. Natl. Acad. Sci. USA.* 111:5652–5657. http://dx.doi.org/10.1073/pnas.1321803111

Honda, T., J.G. Egen, T. Lämmermann, W. Kastenmüller, P. Torabi-Parizi, and R.N. Germain. 2014. Tuning of antigen sensitivity by T cell receptor-dependent negative feedback controls T cell effector function in inflamed tissues. *Immunity.* 40:235–247. http://dx.doi.org/10.1016/j.immuni.2013.11.017

Johnston, R.J., A.C. Poholek, D. DiToro, I. Yusuf, D. Eto, B. Barnett, A.L. Dent, J. Craft, and S. Crotty. 2009. Bcl6 and Blimp-1 are reciprocal and antagonistic regulators of T follicular helper cell differentiation. *Science.* 325:1006–1010. http://dx.doi.org/10.1126/science.1175870

Kahnert, A., U.E. Höpken, M. Stein, S. Bandermann, M. Lipp, and S.H. Kaufmann. 2007. *Mycobacterium tuberculosis* triggers formation of lymphoid structure in murine lungs. *J. Infect. Dis.* 195:46–54. http://dx.doi.org/10.1086/508894

Khader, S.A., J. Rangel-Moreno, J.J. Fountain, C.A. Martino, W.W. Reiley, J.E. Pearl, G.M. Winslow, D.L. Woodland, T.D. Randall, and A.M. Cooper. 2009. In a murine tuberculosis model, the absence of homeostatic chemokines delays granuloma formation and protective immunity. *J. Immunol.* 183:8004–8014. http://dx.doi.org/10.4049/jimmunol.0901937

Lázár-Molnár, E., B. Chen, K.A. Sweeney, E.J. Wang, W. Liu, J. Lin, S.A. Porcelli, S.C. Almo, S.G. Nathenson, and W.R. Jacobs Jr. 2010. Programmed death-1 (PD-1)-deficient mice are extraordinarily sensitive to tuberculosis. *Proc. Natl. Acad. Sci. USA.* 107:13402–13407. http://dx.doi.org/10.1073/pnas.1007394107

Leal, I.S., B. Smedegård, P. Andersen, and R. Appelberg. 2001. Failure to induce enhanced protection against tuberculosis by increasing T-cell-dependent interferon-gamma generation. *Immunology.* 104:157–161. http://dx.doi.org/10.1046/j.1365-2567.2001.01305.x

Lindenstrøm, T., N.P. Knudsen, E.M. Agger, and P. Andersen. 2013. Control of chronic *Mycobacterium tuberculosis* infection by CD4 KLRG1- IL-2-secreting central memory cells. *J. Immunol.* 190:6311–6319. http://dx.doi.org/10.4049/jimmunol.1300248

Marshall, H.D., A. Chandele, Y.W. Jung, H. Meng, A.C. Poholek, I.A. Parish, R. Rutishauser, W. Cui, S.H. Kleinstein, J. Craft, and S.M. Kaech. 2011. Differential expression of Ly6C and T-bet distinguish effector and memory Th1 CD4(+) cell properties during viral infection. *Immunity.* 35:633–646. http://dx.doi.org/10.1016/j.immuni.2011.08.016

Mittrücker, H.W., U. Steinhoff, A. Köhler, M. Krause, D. Lazar, P. Mex, D. Miekley, and S.H. Kaufmann. 2007. Poor correlation between BCG vaccination-induced T cell responses and protection against tuberculosis. *Proc. Natl. Acad. Sci. USA*. 104:12434–12439. http://dx.doi.org/10.1073/pnas.0703510104

Mollo, S.B., A.J. Zajac, and L.E. Harrington. 2013. Temporal requirements for B cells in the establishment of CD4 T cell memory. *J. Immunol.* 191:6052–6059. http://dx.doi.org/10.4049/jimmunol.1302033

Moon, J.J., H.H. Chu, M. Pepper, S.J. McSorley, S.C. Jameson, R.M. Kedl, and M.K. Jenkins. 2007. Naive CD4(+) T cell frequency varies for different epitopes and predicts repertoire diversity and response magnitude. *Immunity*. 27:203–213. http://dx.doi.org/10.1016/j.immuni.2007.07.007

Moon, J.J., H.H. Chu, J. Hataye, A.J. Pagán, M. Pepper, J.B. McLachlan, T. Zell, and M.K. Jenkins. 2009. Tracking epitope-specific T cells. *Nat. Protoc.* 4:565–581. http://dx.doi.org/10.1038/nprot.2009.9

Nakayamada, S., Y. Kanno, H. Takahashi, D. Jankovic, K.T. Lu, T.A. Johnson, H.W. Sun, G. Vahedi, O. Hakim, R. Handon, et al. 2011. Early Th1 cell differentiation is marked by a Tfh cell-like transition. *Immunity*. 35:919–931. http://dx.doi.org/10.1016/j.immuni.2011.11.012

Nurieva, R.I., Y. Chung, G.J. Martinez, X.O. Yang, S. Tanaka, T.D. Matskevitch, Y.H. Wang, and C. Dong. 2009. Bcl6 mediates the development of T follicular helper cells. *Science*. 325:1001–1005. http://dx.doi.org/10.1126/science.1176676

Oestreich, K.J., A.C. Huang, and A.S. Weinmann. 2011. The lineage-defining factors T-bet and Bcl-6 collaborate to regulate Th1 gene expression patterns. *J. Exp. Med.* 208:1001–1013. http://dx.doi.org/10.1084/jem.20102144

Oestreich, K.J., S.E. Mohn, and A.S. Weinmann. 2012. Molecular mechanisms that control the expression and activity of Bcl-6 in TH1 cells to regulate flexibility with a TFH-like gene profile. *Nat. Immunol.* 13:405–411. http://dx.doi.org/10.1038/ni.2242

Pepper, M., A.J. Pagán, B.Z. Igyártó, J.J. Taylor, and M.K. Jenkins. 2011. Opposing signals from the Bcl6 transcription factor and the interleukin-2 receptor generate T helper 1 central and effector memory cells. *Immunity*. 35:583–595. http://dx.doi.org/10.1016/j.immuni.2011.09.009

Ravn, P., A. Demissie, T. Eguale, H. Wondwosson, D. Lein, H.A. Amoudy, A.S. Mustafa, A.K. Jensen, A. Holm, I. Rosenkrands, et al. 1999. Human T cell responses to the ESAT-6 antigen from *Mycobacterium tuberculosis*. *J. Infect. Dis.* 179:637–645. http://dx.doi.org/10.1086/314640

Reiley, W.W., S. Shafiani, S.T. Wittmer, G. Tucker-Heard, J.J. Moon, M.K. Jenkins, K.B. Urdahl, G.M. Winslow, and D.L. Woodland. 2010. Distinct functions of antigen-specific CD4 T cells during murine Mycobacterium tuberculosis infection. *Proc. Natl. Acad. Sci. USA*. 107:19408–19413. http://dx.doi.org/10.1073/pnas.1006298107

Riley, J.L. 2009. PD-1 signaling in primary T cells. *Immunol. Rev.* 229:114–125. http://dx.doi.org/10.1111/j.1600-065X.2009.00767.x

Rogerson, B.J., Y.J. Jung, R. LaCourse, L. Ryan, N. Enright, and R.J. North. 2006. Expression levels of Mycobacterium tuberculosis antigen-encoding genes versus production levels of antigen-specific T cells during stationary level lung infection in mice. *Immunology*. 118:195–201. http://dx.doi.org/10.1111/j.1365-2567.2006.02355.x

Sakai, S., K.D. Kauffman, J.M. Schenkel, C.C. McBerry, K.D. Mayer-Barber, D. Masopust, and D.L. Barber. 2014. Cutting edge: control of *Mycobacterium tuberculosis* infection by a subset of lung parenchyma-homing CD4 T cells. *J. Immunol.* 192:2965–2969. http://dx.doi.org/10.4049/jimmunol.1400019

Sallusto, F., A. Lanzavecchia, K. Araki, and R. Ahmed. 2010. From vaccines to memory and back. *Immunity*. 33:451–463. http://dx.doi.org/10.1016/j.immuni.2010.10.008

Schreiber, S.L., and G.R. Crabtree. 1992. The mechanism of action of cyclosporin A and FK506. *Immunol. Today*. 13:136–142. http://dx.doi.org/10.1016/0167-5699(92)90111-J

Scriba, T.J., M. Tameris, N. Mansoor, E. Smit, L. van der Merwe, K. Mauff, E.J. Hughes, S. Moyo, N. Brittain, A. Lawrie, et al. 2011. Dose-finding study of the novel tuberculosis vaccine, MVA85A, in healthy BCG-vaccinated infants. *J. Infect. Dis.* 203:1832–1843. http://dx.doi.org/10.1093/infdis/jir195

Shafiani, S., G. Tucker-Heard, A. Kariyone, K. Takatsu, and K.B. Urdahl. 2010. Pathogen-specific regulatory T cells delay the arrival of effector T cells in the lung during early tuberculosis. *J. Exp. Med.* 207:1409–1420. http://dx.doi.org/10.1084/jem.20091885

Shafiani, S., C. Dinh, J.M. Ertelt, A.O. Moguche, I. Siddiqui, K.S. Smigiel, P. Sharma, D.J. Campbell, S.S. Way, and K.B. Urdahl. 2013. Pathogen-specific Treg cells expand early during *Mycobacterium tuberculosis* infection but are later eliminated in response to Interleukin-12. *Immunity*. 38:1261–1270. http://dx.doi.org/10.1016/j.immuni.2013.06.003

Slight, S.R., J. Rangel-Moreno, R. Gopal, Y. Lin, B.A. Fallert Junecko, S. Mehra, M. Selman, E. Becerril-Villanueva, J. Baquera-Heredia, L. Pavon, et al. 2013. CXCR5$^+$ T helper cells mediate protective immunity against tuberculosis. *J. Clin. Invest.* 123:712–726. http://dx.doi.org/10.1172/JCI65728

Srivastava, S., and J.D. Ernst. 2014. Cell-to-cell transfer of M. tuberculosis antigens optimizes CD4 T cell priming. *Cell Host Microbe*. 15:741–752. http://dx.doi.org/10.1016/j.chom.2014.05.007

Tameris, M.D., M. Hatherill, B.S. Landry, T.J. Scriba, M.A. Snowden, S. Lockhart, J.E. Shea, J.B. McClain, G.D. Hussey, W.A. Hanekom, et al. MVA85A 020 Trial Study Team. 2013. Safety and efficacy of MVA85A, a new tuberculosis vaccine, in infants previously vaccinated with BCG: a randomised, placebo-controlled phase 2b trial. *Lancet*. 381:1021–1028. http://dx.doi.org/10.1016/S0140-6736(13)60177-4

Urdahl, K.B. 2014. Understanding and overcoming the barriers to T cell-mediated immunity against tuberculosis. *J. Immunol.* 170:1987–1994. http://dx.doi.org/10.1016/j.smim.2014.10.003

Urdahl, K.B., D. Liggitt, and M.J. Bevan. 2003. CD8+ T cells accumulate in the lungs of *Mycobacterium tuberculosis*-infected $K^{b-/-}D^{b-/-}$ mice, but provide minimal protection. *Mucosal Immunol.* 170:1987–1994. http://dx.doi.org/10.4049/jimmunol.170.4.1987

Urdahl, K.B., S. Shafiani, and J.D. Ernst. 2011. Initiation and regulation of T-cell responses in tuberculosis. *Mucosal Immunol.* 4:288–293. http://dx.doi.org/10.1038/mi.2011.10

WHO. 2014. Global tuberculosis report 2014. In Geneva. World Health Organization

Winslow, G.M., A.D. Roberts, M.A. Blackman, and D.L. Woodland. 2003. Persistence and turnover of antigen-specific CD4 T cells during chronic tuberculosis infection in the mouse. *J. Immunol.* 170:2046–2052. http://dx.doi.org/10.4049/jimmunol.170.4.2046

Woodworth, J.S., C.S. Aagaard, P.R. Hansen, J.P. Cassidy, E.M. Agger, and P. Andersen. 2014. Protective CD4 T cells targeting cryptic epitopes of *Mycobacterium tuberculosis* resist infection-driven terminal differentiation. *J. Immunol.* 192:3247–3258. http://dx.doi.org/10.4049/jimmunol.1300283

Yu, D., S. Rao, L.M. Tsai, S.K. Lee, Y. He, E.L. Sutcliffe, M. Srivastava, M. Linterman, L. Zheng, N. Simpson, et al. 2009. The transcriptional repressor Bcl-6 directs T follicular helper cell lineage commitment. *Immunity*. 31:457–468. http://dx.doi.org/10.1016/j.immuni.2009.07.002